Indonesian Journal of Aerospace Vol. 24 No. 1 June 2026 : pp 61–72 (Rohman et al.)
DOI: 10.55981/ijoa.2026.16098
https://ejournal.brin.go.id/ijoa/

Sharp Roll-Off Microstrip Low-Pass Filter with Transmission Zero Using SIR Stub T-Shaped for C-Band Synthetic Aperture Radar Transceivers UAV Payload

Abdul Rohman[1], Catur Apriono[1*], Farohaji Kurniawan[2], Satria Arief Aditya[1,2]

[1]Department of Electrical Engineering, Faculty of Engineering, Universitas Indonesia, Depok, West Java, 16424, Indonesia
[2]Research Center for Aeronautics Technology - National Research and Innovation Agency (BRIN), Bogor, West Java, 16350, Indonesia
*e-mail: catur@eng.ui.ac.id

Received:26/11/2025 Revised: 23/01/2026 Accepted: 29/01/2026 Published: 26/10/2026)

Abstract

This paper presents the design and experimental realization of a 5th-order Chebyshev microstrip low-pass filter (LPF) based on a Stepped Impedance Resonator (SIR) integrating T-shaped stub topology at center frequency (fc) 5.575 GHz for synthetic aperture radar (SAR) system applications. Two topologies are systematically compared: conventional SIR and SIR T-shaped stub (SIRS T-Shaped), and both are fabricated on Rogers 5880 substrate. The simulation was conducted using two electromagnetic simulations as perform cross-validation. The measurement results show that the SIRS-T topology achieves insertion loss (IL) S21 of -4.67 dB at the center frequency with a transmission zero (Tz) depth of -61.46 dB at 12.24 GHz, while the conventional SIR yields IL S21 of -8.2 dB, well beyond the acceptable degradation threshold. The deviation may be attributed to practical factors such as fabrication tolerances, conductor and dielectric losses, soldering effects of SMA connectors, and parasitic discontinuities introduced by the embedded T-shaped structure. The SIRS-T structure demonstrates clear superiority in harmonic suppression and roll-off sharpness, establishing it as the preferred LPF architecture for C-band SAR for UAV payload applications.

Keywords: low-pass filter; sir; t-shaped; transmission zero; synthetic aperture radar

1. Introduction

Synthetic Aperture Radar (SAR) is a high-resolution remote sensing radar technology capable of operating under various weather and illumination conditions (Micallef, Gu, & Wu, 2024). Due to its continuous advancements, SAR has been widely employed in both civilian and military applications as UAV payload, including land monitoring (Geng, Ma, Fan, & Wang, 2018), land deformation (Sri Sumantyo, Shimada, Mathieu, & Abidin, 2012), disaster management analysis (Bignami et al., 2013; Tomiyama, Koike, & Omura, 2004), target detection (Cao, Zhao, Dong, & Fu, 2024; Wang, Shi, Liu, Zhao, & Kuang, 2012), and border surveillance (Appleby et al., 2021; Cope, Tougher, Morten, Pukini, & Zetterlind, 2022). Therefore, high reliability and robust performance of the radio frequency (RF) system are critically required.

The low-pass filter is a critical component in the SAR (Synthetic Aperture Radar) transceiver system, as it must suppress harmonic frequency aliasing that directly degrades radar image quality. In C-band SAR systems operating near 5.5 GHz, the LPF must exhibit a sharp cutoff response accompanied by a minimum stopband (SB) attenuation of -40 dB to give a guaranteed signal integrity at the receiver input. The failure to suppress harmonic components at 2 times of the center frequency (2fc) affects the signal-to-noise ratio (SNR) and azimuth resolution of the radar directly, ultimately producing image artifacts. Accordingly, LPF designs exhibiting deep transmission zeros and sharp roll-off are non-negotiable technical requirements in modern SAR platforms.

e-ISSN 2597-7873 (online) | © 2026 The Author(s). Published by BRIN Publishing.
This is an open access article under the CC BY-SA license(https://creativecommons.org/licenses/by-sa/4.0/)
IJOA accredited as Sinta 2 Journal (https://sinta.kemdikbud.go.id/journals/profile/3362)

In the past, extensive studies have been conducted on LPF based on SIR. To achieve wider stopband characteristics and enhance Tz, various resonator modifications have been introduced, including spiral resonators (Majidifar, Makki, Ahmadi, & Alirezaee, 2012), hairpin structures (F. Zhang, Gao, Liu, & Xu, 2020). In addition, defected ground structure (DGS) techniques have demonstrated excellent performance in improving stopband bandwidth and transmission-zero generation (Liu, Yu, & Liu, 2019; Vali & Rao, 2024; J. Zhang, Yang, & Zhang, 2019). Nevertheless, these approaches commonly require ground-plane modification and double-sided fabrication processes, resulting in increased manufacturing complexity and implementation difficulty.

The T-shaped stub approach as a single-sided alternative was reported. In (Hayati, Salahi, Akbari, Zargari, & Abbott, 2023) a T-shaped topology combined with open-stub suppressor cells achieved an S21 of only -0.37 dB at a cutoff frequency of 1.52 GHz. Meanwhile, the work in (Ouf, El-Hameed, & Abdallah, 2024) targeted a cutoff frequency of 3.4 GHz and achieved a transmission-zero depth of approximately -55 dB with an S21 of -0.7 dB. Nevertheless, most reported designs rely on multiple resonators or multiple suppressor cells to generate several transmission zeros and realize ultra-wide stopband characteristics. Such additions inevitably increase structural and fabrication complexity. Therefore, a simpler LPF topology capable of generating deep transmission zeros and enhanced stopband performance without employing multi-resonator configurations, multiple suppressor cells, or DGS implementation remains highly desirable.

This paper presents the design, simulation, fabrication, and experimental validation of a low-pass filter based on an SIR loaded with a T-shaped stub (SIRS-T Shaped). The proposed approach aims to address the fundamental limitations in achieving a -40 dB stopband attenuation level and sharp transmission-zero characteristics while maintaining a simple structure without extensive resonator or ground-plane modifications.

2. Filter Design and Synthesis

The low-pass filter specifications considered in this study are presented in Table 2-1. As seen, the proposed filter was synthesized of a fifth-order Chebyshev with 0.1 dB passband ripple and cutoff frequency fc = 5.575 GHz. The design employed a high-impedance section (Z_H) of 100 Ω and a low-impedance (Z_L) of 20 Ω. The target performance is the insertion loss S21 greater than -3 dB and the return loss S11 lower than -15 dB. The filter is implemented on a Rogers RT/Duroid 5880 substrate with a thickness (h) of 0.508 mm, relative permittivity (εr) of 2.2, and loss tangent (tan δ) of 0.0009.

Table 2-1: LPF Specifications

Parameter	Symbol	Value
Cut-off frequency	fc	5.575 GHz
Stopband Attenuation	SB	-40 dB
Passband Ripple	Lar	0.1 dB
Filter order	N	5
Input impedances	Z0	50 Ω
High impedances	Z_H	100 Ω
Low impedances	Z_L	20 Ω
S21 Cutoff	IL	≥ -5 dB
S11 Cutoff	RL	≤ -15 dB

A LPF prototype with a passband ripple of 0.1 dB is adopted as the initial design model, the values of the lumped-element prototype can be calculated using Eq. (2-1) and Eq. (2-2). The denormalized coefficients *gn* are obtained from Table 2-2 (Pozar, 2012).

$$L = \frac{Z_0\, g_n}{2\pi f_c} \tag{2-1}$$

$$C = \frac{g_n}{2\pi f_c Z_0} \tag{2-2}$$

The proposed low-pass filter (LPF) is synthesized using the stepped-impedance technique, in which high-impedance transmission lines emulate inductive elements, while low-impedance transmission lines emulate capacitive elements (Hong & Lancaster, 2011). For electrically short transmission lines θ less than 30 degrees, the approximation $\sin\theta \approx \theta$ can be applied, resulting in simplified equivalent lumped elements. Accordingly, the equivalent inductance and capacitance can be expressed as Eq. (2-3) and Eq. (2-4).

Table 2-2: Denormalized Inductance and Capacitance Values

gn	Element	Value
1.1468	L1=L5	1.637 nH
1.3712	C2=C4	0.783 pF
1.9750	L3	2.819 nH

$$L = \frac{Z_H\, \theta_H}{2\pi f_c} \tag{2-3}$$

$$C = \frac{\theta_L}{2\pi f_c Z_L} \tag{2-4}$$

where Z_H and Z_L denote the characteristic impedances of the high and low-impedance sections, respectively, θ_H and θ_L are the corresponding electrical lengths, and ω_c is the cutoff angular. The proposed LPF employs a high-impedance section of 100 Ω and a low-impedance section of 20 Ω, resulting in an impedance ratio defined as Eq. (2-5) below.

$$K = \frac{Z_H}{Z_L} \tag{2-5}$$

For the proposed design, K = 100/20 = 5. A larger impedance ratio generally improves the LPF characteristics by increasing the contrast between the equivalent inductive and capacitive sections. In addition, it shifts spurious resonances toward higher frequencies, thereby enhancing harmonic suppression and extending the effective stopband region (Hong & Lancaster, 2011). To further improve stopband performance, an open-circuit stub is incorporated into the conventional stepped-impedance resonator (SIR). The input impedance of the open-circuit stub is given by (Collin, 1992)

$$Z_{stub} = -jZ_0 \cot(\beta l) \tag{2-6}$$

where Z_0 is the characteristic impedance of the stub, βl is the electrical length equal a half of $(2n+1)\pi$ $(2n+1)\pi$ and l is the physical length defined by Eq. (2-7) below.

$$l = \frac{\beta l \, \lambda_g}{2\pi} \tag{2-7}$$

The physical dimensions of the proposed low-pass filter are presented in Table 2-3. The microstrip dimensions were determined based on the guided wavelength λ_g, associated with each impedance section and subsequently refined through electromagnetic optimization to satisfy the target cutoff frequency of 5.575 GHz. For the capacitive transmission line section Z_L = 20 Ω, WC = 5.05 mm, the guided wavelength was calculated $\lambda_g C$ = 38.29 mm, lengths l1 = l5 = 2.90 mm and l2 = l4 = 4.94 mm as proportional fractions of $\lambda_g C/4$. For the inductive trace Z_H = 100 Ω, WL = 0.455 mm, the guided wavelength $\lambda_g L$ = 41.13 mm produces the central resonator element l3 = 5.54 mm, functioning as the third-order series inductive resonator.

Table 2-3: Physical Dimensions of the Proposed SIR LPF

Parameter	Symbol	Width (mm)
Outer Section	l1=l5	2.90
Intermediate Section	l2=l4	4.94
Center Section	l3	5.54
T-shaped Parameter	Width (mm)	Length (mm)
Vertical Square	2	1
Horizontal Square	0.4	1.5

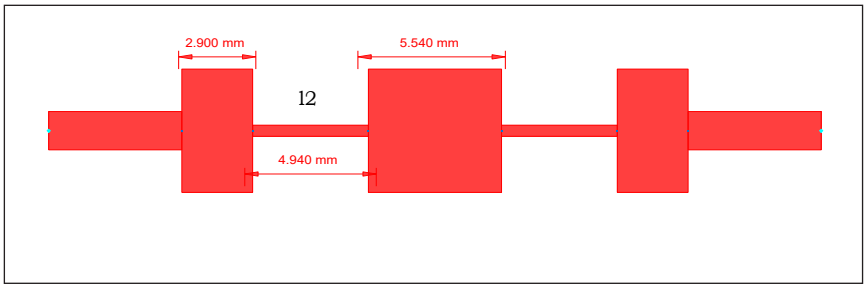


Figure 2-1: The schematic view LPF SIR Conventional.

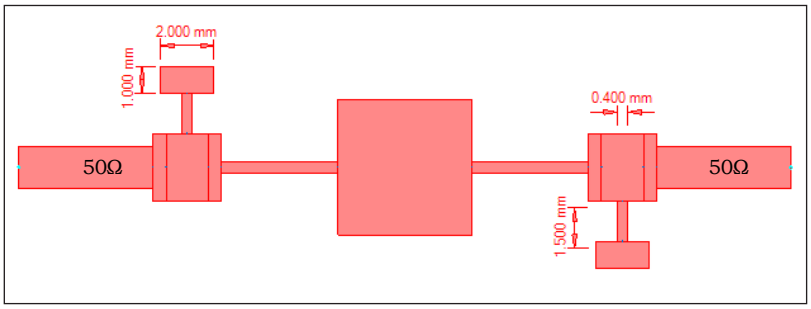


Figure 2-2: The schematic view LPF SIRS T-shaped.

Figure 2-1 shows the geometry of the conventional stepped impedance resonator (SIR), which is symmetric about the central section l3. The proposed transformed stepped impedance resonator with a loaded stub T-shaped is shown in Figure 2-2. The topology transformation from conventional SIR to T-shaped SIRS is realized by embedding the single shunt resonator

at positions l1 and l5 with a pair of parallel stubs forming a T-junction configuration with dimensions of 2 mm x 1 mm. Each T-shaped stub possesses an electrical length of $\lambda_g C/4$ at frequency 2fc, thereby inducing a transmission zero via open-circuit parallel resonance at the target stopband frequency.

3. Result and Analysis

The fabricated prototypes were measured at the Payload and Aerosense Laboratory, Research Center for Aeronautics Technology, National Research and Innovation Agency (BRIN), using the negative photoresist method. S-parameter characterization was performed using Keysight N9917A Vector Network Analyzer (VNA). Prior to measurement, the VNA was calibrated using the Short-Open-Load-Thru (SOLT) technique over the frequency range of 0–18 GHz to minimize systematic measurement errors.

Figures 3-1 and 3-2 illustrate the experimental setup used for S-parameter characterization. The return loss S11 measurement was conducted by terminating the output port with a matched 50 Ω load to ensure proper impedance matching during the reflection measurement. The insertion loss S21 measurement was performed using two ports through configuration, where both ports of the filter were connected directly to the VNA.

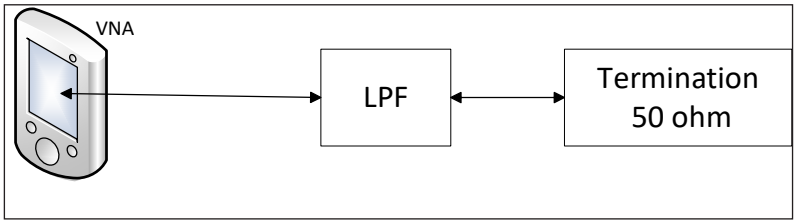


Figure 3-1: Measurement Configuration Return Loss S11.

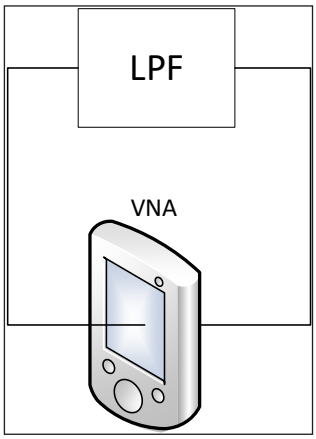


Figure 3-2: Measurement Configuration Insertion Loss S21.

Figure 3-3 (a) and (b) presents the fabricated conventional SIR and proposed SIRS-T LPF. Both prototypes were implemented on a Rogers RT/duroid 5880 substrate with identical dimensions of 28 mm × 16 mm, ensuring that performance differences are solely attributed to the incorporation of the T-shaped stubs.

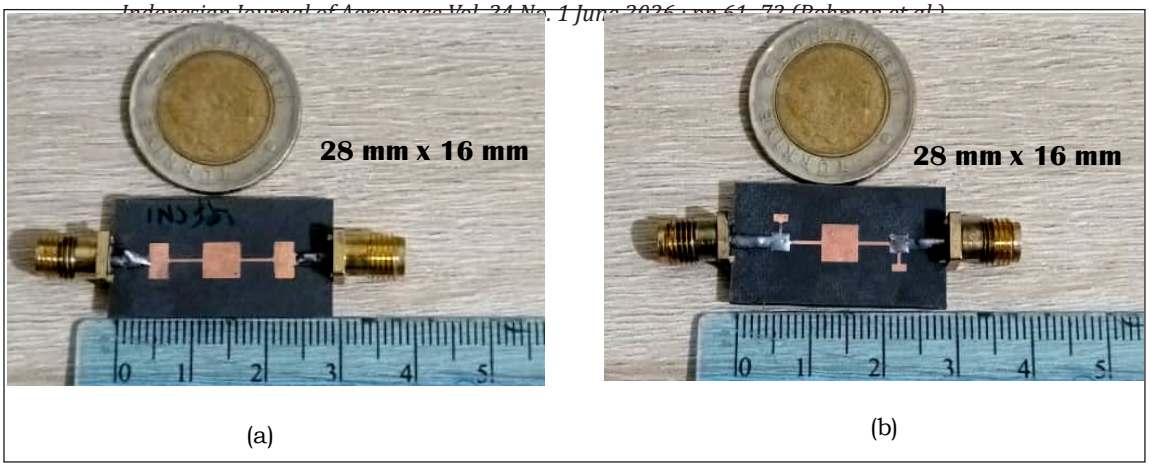


Figure 3-3: (a) SIR Conventional LPF Fabrication (b) SIRS T-Shaped LPF Fabrication.

This study was simulated using two full-wave electromagnetic (EM) Simulator tools, Keysight ADS (Simulator 1) and CST Studio Suite (Simulator 2), to implement a cross-validation approach. CST Studio Suite employs three-dimensional (3D) electromagnetic simulation techniques, such as the Finite Integration Technique (FIT) and Finite Difference Time Domain (FDTD) methods. In contrast, Keysight ADS utilizes circuit-based approaches, including nodal analysis, as well as planar electromagnetic methods such as the Method of Moments (MoM). Both simulation platforms offer their own advantages and unique capabilities depending on the analysis requirements. The insertion loss (IL) response, represented by S21, and the return loss (RL) response, represented by S11, are presented separately in Figure 3-4 and Figure 3-5 to improve readability and facilitate analysis. In the presented curves, the red line corresponds to Simulator 1, while the blue line represents Simulator 2.

Figure 3-4 presents the return loss and insertion loss responses of the conventional SIR LPF, respectively. For S11 response at -15 dB, both simulation results indicate frequencies above 4.7 GHz, while the measured result shows a slightly shifted response at 4.64 GHz. Regarding stopband performance at the -40 dB attenuation level, the conventional SIR does not exhibit a stopband response reaching such attenuation. In terms of transmission zero characteristics, the measurement result demonstrates a transmission zero magnitude of -26.82 dB.

Meanwhile, Figure 3-5 shows the corresponding return loss and insertion loss characteristics of the proposed SIRS T-shaped LPF. A comparison of the S-parameter responses reveals fundamental differences between the two topologies in terms of both passband performance and stopband characteristics. In contrast, both simulators produced good results, with S21 of -2.93 dB and -2.76 dB, respectively. The transmission-zero response also showed significant improvement, reaching below -50 dB for both simulators, which is much better than that of the conventional SIR. Experimentally, the T-shaped SIRS achieved S21 -4.67 dB at fc, accompanied by Tz of -61.46 dB at 12.24 GHz. This result effectively suppresses the second harmonic far beyond the -40 dB target. Furthermore, the S11 response confirms superior passband matching, with S11 lower than -15 dB maintained across the frequency range up to fc. The -40 dB stopband attenuation point was observed at 11.89 GHz.

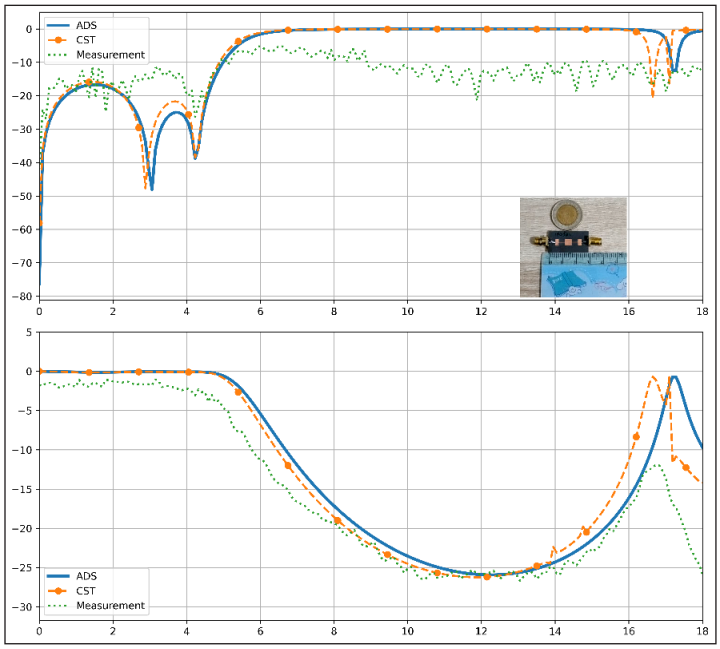


Figure 3-4: Measurement Results (a) Reflection Loss S11 and Insertion Loss S21 (b) Fabrication SIRS Conventional.

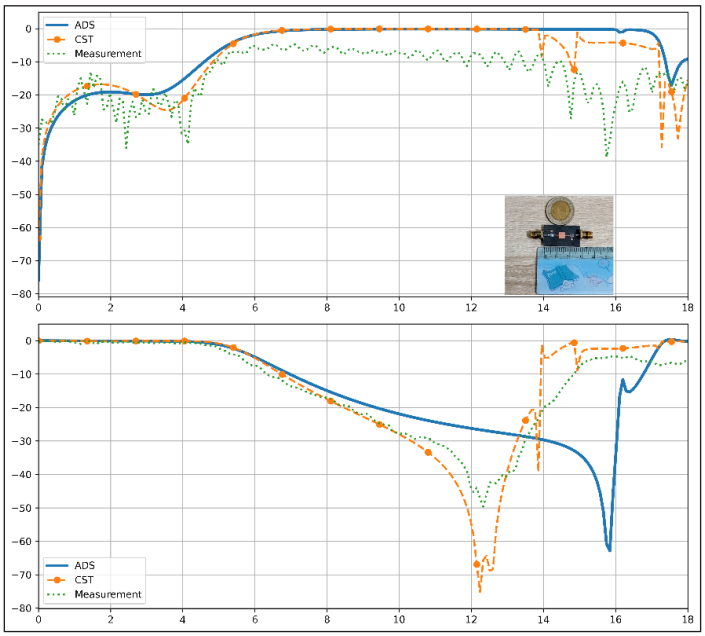


Figure 3-5: Measurement Results (a) Reflection Loss S11 and Insertion Loss S21 (b) Fabrication SIRS T-Shaped.

In addition to the physical layout parameters, it is also worth noting a minor discrepancy in the transmission zero (Tz) location between the two software solvers. Simulator 1, which utilizes a circuit-planar 2.5D Method of Moments (MoM) approach, identifies the Tz at a slightly shifted frequency compared to the 3D full-wave Finite Integration Technique (FIT) employed in Simulator 2. This variance is a well-understood consequence of the differing numerical algorithms, particularly in how each simulator defines localized mesh densities, port excitation

setups, and the mathematical approximations of open boundary conditions within planar versus full-wave 3D computational environments.

Table 3-1: Performance of SIR Conventional versus SIRS T-Shaped LPF

	Topology of LPF	**Parameters**			
		S11 -15dB (@ GHz)	**S21 fc (dB)**	**BS -40 dB (@ GHz)**	**Tz (dB)**
Simulator 1	SIR Conventional	4.70	-3.90	-	-39.81 @13.92 GHz
	SIRS T-Shaped	4.43	-2.93	11.55	-80.23 @ 12.33 GHz
Simulator 2	SIR Conventional	4.74	-2.76	-	-25.92 @ 12.25 GHz
	SIRS T-Shaped	4.05	-2.97	15.41	-66.73 @15.80 GHz
Measurement	SIR Conventional	4.64	-8.20	-	-26.82 @ 10.89 GHz
	SIRS T-Shaped	4.58	-4.67	11.89	-61.46 @ 12.24 GHz

To further investigate the underlying causes of the simulation to measurement gap, a qualitative and quantitative loss analysis was performed. The observed degradation in the measured insertion loss S21 is primarily caused by three cumulative practical factors. First, the sub-miniature version SMA connectors soldered to the microstrip ports introduce an inevitable residual insertion loss, typically ranging from 0.1 to 0.2 dB per port, which inherently accounts for a 0.2 to 0.4 dB drop across the passband. Second, at high C-band frequencies, the skin effect confines the signal current to a very thin superficial layer of the conductor. This phenomenon renders the filter's performance highly susceptible to the copper surface roughness of the Rogers 5880 substrate, thereby elevating the planar resistance and introducing additional attenuation. Lastly, minor dimensional deviations during the chemical wet-etching fabrication process such as a 20–50 μm erosion along the microstrip line edge slightly alter the physical geometry of the SIRS-T structure, shifting the characteristic impedance from its nominal value and contributing to the overall mismatch.

Table 3-1 tabulates the overall performance comparison of the conventional SIR and the proposed SIRS T-shaped structures. From the S-parameter performance, S21 in Simulator 1 indicates that the filter does not satisfy the target specification, whereas Simulator 2 demonstrates that the filter achieves the required response below -3 dB at the cutoff frequency. A discrepancy between the two simulation platforms is observed, with a deviation of approximately -1.2 dB. Experimentally, the conventional SIR exhibits an S21 of -8.2 dB at 5.575 GHz.

Table 3-2 summarizes the characteristics of some published lowpass filters. As can be seen from the table, our proposed filter has the properties of compact size, simple circuit topology, and ultra-wide stopband among the quoted filters. The proposed filter demonstrates a distinctive high-frequency transition profile at the C-band spectrum by achieving a balanced Figure of Merit (FoM) Ω_{SB} of 2.13. While lower-frequency reference filters, such as those by *(Hayati et al., 2023)* (Ω_{SB} = 1.11), *(J. Zhang et al., 2019)* (Ω_{SB} = 1.21), and *(Majidifar et al., 2012)* (Ω_{SB} = 1.21), yield tighter fractional transitions, their topologies are strictly constrained to operations below 2.3 GHz. Maintaining a sharp selectivity roll-off becomes significantly more challenging at higher operating frequencies due to parasitic coupling effects and increased

radiation losses. Compared to the conventional C-band SIR design, which suffers from an unselective transmission skirt and a severe insertion loss of -8.2 dB at fc the introduced T-shaped stub loading effectively sharpens the frequency response, optimizing the insertion loss to 4.67 dB while shifting the ultimate stopband rejection deep into the higher spectrum.

A critical limitation observed in many planar LPFs is the shallow suppression depth within the stopband region, where the out-of-band rejection of the flexible LPF by Liu et al. only reaches -15 dB, while the design by J. Zhang et al. hovers around the -20 dB threshold. Such low suppression levels fail to effectively eliminate harmonic interferences in modern high-power RF front-ends. The proposed SIRS-T filter significantly outperforms these reference designs by achieving an exceptionally deep and stable harmonic suppression level of -40 dB. This performance is driven by the generation of a deep transmission zero Tz located at 12.24 GHz, yielding an extreme attenuation floor of -61.46 dB. This out-of-band rejection profile ensures complete suppression of the second harmonic 2fc = 11.15 GHz, which is a crucial requirement to protect the signal integrity of C-band Synthetic Aperture Radar (SAR) UAV transceivers from transmitter harmonics.

Table 3-2: Characteristic Comparison Among Published Filters and The Proposed One

Ref.	fc (GHz)	S21 fc (dB)	SB Atten. (dB)	fTz (GHz)	Tz (dB)	FoM (Ω_{SB})	Subst	Topology
(F. Zhang et al., 2020)	1.52	-0.37	-20	2.12	-50	1.5	RT/duroid 5880	SIR Hairpin + Stub Square
(Ouf et al., 2024)	3.4	-0.7	-20	3.9	-55	1.09	RT/duroid 4003C	Tshaped resonator+ open Stub+ DGS
(Vali & Rao, 2024)	14	-0.2	-29	-	-	1.16	RT/duroid 4003C	CPW + Triangle DGS
(Majidifar et al., 2012)	2.28	-0.38	-20	2.75	-45	1.21	PTPE composite substrate	SIR + Three DGS Units
(J. Zhang et al., 2019)	2	-0.3	-20	2.15	-67	1.21	RT/duroid 5880	SIR + 3-DGS
(Hayati et al., 2023)	2.15	-1	-25	-	-	1.11	Panasonic R-F775 Polyimide	SIR + Tshaped
(Liu et al., 2019)	7	-3	-15	2.78	-32.56	1.33	RT/duroid 5880	SIR+Spiral Rectangular
This Work (Conv. SIR)	5.575	-8.2	< -20	-	-	-	RT/duroid 5880	SIR 5th
This Work (SIRS-T)	5.575	-4.67	-40	12.24	-61.46	2.13	RT/duroid 5880	SIR T-Shaped Stub

From a structural perspective, the majority of the reported works with high rejection metrics heavily rely on Defected Ground Structures (DGS) to broaden the stopband, as seen in the designs by *(Liu et al., 2019; Majidifar et al., 2012; F. Zhang et al., 2020)*. Although etching slots onto the ground plane provides additional equivalent inductance, it increases vulnerability to backward radiation leakage and requires a dedicated air cavity beneath the PCB layer, which violates the strict packaging limits of lightweight UAV payloads. The proposed SIRS-T design, matching the topological philosophy of (Hayati et al., 2023), completely bypasses these constraints by utilizing a solid, un-defected ground plane. All resonant tuning and suppression characteristics are engineered strictly on the top conductor layer, providing robust electromagnetic shielding and permitting direct, flush-mounting onto the metallic chassis of UAV radar housing without performance degradation.

4. Conclusions

This paper experimentally demonstrates a low-pass filter based on a stepped impedance resonator with a T-shaped (SIRS T-Shaped), addressing the fundamental limitations of the conventional SIR in C-band SAR applications at 5.575 GHz. A fifth-order prototype of the SIR conventional and the embedded SIRS T-Shaped structure has been simulated by two electromagnetic solvers and subsequently measured. The results show that the conventional SIR fails to maintain experimental S21 > -3 and does not achieve -40 dB stopband attenuation. In contrast, the proposed SIRS-T achieves a transmission-zero depth of -61.46 dB at 12.24 GHz, exceeding the -40 dB requirement by -21.46 dB, while maintaining S21 = -4.67 dB at fc. This deviation may be attributed to practical factors for future such as fabrication tolerances, conductor and dielectric losses, soldering effects of SMA connectors, and parasitic discontinuities introduced by the embedded T-shaped structure. This performance gap indicates that the T-stub configuration is not merely a geometric modification, but a substantial enhancement of the transmission-zero generation and stopband suppression mechanism in SIR low-pass filter design.

5. Acknowledgements

This research was supported by the Directorate of Research and Community Service (Direktorat Penelitian dan Pengabdian kepada Masyarakat), Directorate General of Research and Development, Ministry of Higher Education, Science, and Technology of the Republic of Indonesia through the Program Bantuan Operasional Perguruan Tinggi Negeri (BOPTN), Program Penelitian Baru - Master's Thesis Research Scheme (Program Penelitian Baru Skema Penelitian Tesis Magister, PPS-PTM), under Research Contract No. PKS-201/UN2.RST/HKP.05.00/2026.

6. Contributorship Statement

AR: Conceptualization, methodology, simulation, fabrication, measurement, data analysis, writing original draft. CA: Supervision, validation, writing review & editing. FK: Supervision, validation, writing review & editing. SAA: Investigation and measurement.

7. References

Appleby, T., Studley, M., Moorhouse, B., Brown, J., Staddon, C., & Bean, E. (2021). Sea of possibilities: Old and new uses of remote sensing data for the enforcement of the Ascension Island marine protected area. *Marine Policy*, *127*, 103184. https://doi.org/10.1016/j.marpol.2018.06.012

Bignami, C., Ruch, J., Chini, M., Neri, M., Buongiorno, M. F., Hidayati, S., … Surono. (2013). Pyroclastic density current volume estimation after the 2010 Merapi volcano eruption using X-band SAR. *Journal of Volcanology and Geothermal Research*, *261*, 236–243. https://doi.org/10.1016/j.jvolgeores.2013.03.023

Cao, S., Zhao, C., Dong, J., & Fu, X. (2024). Ship Detection in Synthetic Aperture Radar Images under Complex Geographical Environments, Based on Deep Learning and Morphological Networks. *Sensors*, *24*(13), 4290. https://doi.org/10.3390/s24134290

Collin, R. E. (1992). *Foundations for Microwave Engineering* (2nd ed.). New York, NY, USA: McGraw-Hill.

Cope, S., Tougher, B., Morten, J., Pukini, C., & Zetterlind, V. (2022). Coastal radar as a tool for continuous and fine-scale monitoring of vessel activities of interest in the vicinity of marine protected areas. *PLOS ONE*, *17*(7), e0269490. https://doi.org/10.1371/journal.pone.0269490

Geng, J., Ma, X., Fan, J., & Wang, H. (2018). Semisupervised Classification of Polarimetric SAR Image via Superpixel Restrained Deep Neural Network. *IEEE Geoscience and Remote Sensing Letters*, *15*(1), 122–126. https://doi.org/10.1109/LGRS.2017.2777450

Hayati, M., Salahi, R., Akbari, M., Zargari, S., & Abbott, D. (2023). Low Complexity Compact Lowpass Filter Using T-Shaped Resonator Loaded With a Stub. *IEEE Access*, *11*, 35763–35769. https://doi.org/10.1109/ACCESS.2023.3263794

Hong, J. S., & Lancaster, M. J. (2011). *Microstrip Filters for RF/Microwave Applications* (2nd ed.). Hoboken, NJ, USA: Wiley.

Liu, S., Yu, C., & Liu, Y. (2019). Optimized design of the flexible stepped impedance lowpass filter based on defected ground structure. *2019 IEEE 6th International Symposium on Electromagnetic Compatibility (ISEMC)*, 1–3. IEEE. https://doi.org/10.1109/ISEMC48616.2019.8986105

Majidifar, S., Makki, S. V. A.-D., Ahmadi, A., & Alirezaee, S. (2012). Compact Microstrip Lowpass Filter Using Stepped Impedance Spiral Resonator. *2012 4th International Conference on Computational Intelligence and Communication Networks (CICN)*, 23–26. IEEE. https://doi.org/10.1109/CICN.2012.64

Micallef, T., Gu, X., & Wu, K. (2024). Resolution Enhancement of Radar Systems through Super Fusion of Non-Contiguous Frequency Bands. *2024 21st European Radar Conference, EuRAD 2024*, 356–359. IEEE. https://doi.org/10.23919/EuRAD61604.2024.10734957

Ouf, E. G., El-Hameed, A. S. A., & Abdallah, E. A. F. (2024). Compact lowpass filter with vast out-of-band rejection utilizing DGS. *AEU - International Journal of Electronics and Communications*, *177*, 155207. https://doi.org/10.1016/j.aeue.2024.155207

Pozar, D. M. (2012). *Microwave Engineering* (4th ed.). Hoboken, NJ, USA: Wiley.

Sri Sumantyo, J. T., Shimada, M., Mathieu, P.-P., & Abidin, H. Z. (2012). Long-Term Consecutive DInSAR for Volume Change Estimation of Land Deformation. *IEEE Transactions on Geoscience and Remote Sensing*, *50*(1), 259–270. https://doi.org/10.1109/TGRS.2011.2160455

Tomiyama, N., Koike, K., & Omura, M. (2004). Detection of topographic changes associated with volcanic activities of Mt. Hossho using D-InSAR. *Advances in Space Research*, *33*(3), 279–283. https://doi.org/10.1016/S0273-1177(03)00483-6

Vali, S. K. S., & Rao, K. S. (2024). Design of wide stopband lowpass filter using defected ground structure. *Microsystem Technologies*, *30*(6), 721–728. https://doi.org/10.1007/s00542-024-05651-w

Wang, N., Shi, G., Liu, L., Zhao, L., & Kuang, G. (2012). Polarimetric SAR Target Detection Using the Reflection Symmetry. *IEEE Geoscience and Remote Sensing Letters*, *9*(6), 1104–1108. https://doi.org/10.1109/LGRS.2012.2189548

Zhang, F., Gao, Y., Liu, B., & Xu, J. (2020). A Compact Sharp Roll-Off Microstrip Lowpass Filter With Ultra-Wide Stopband. *2020 International Conference on Microwave and Millimeter Wave Technology (ICMMT)*, 1–3. IEEE. https://doi.org/10.1109/ICMMT49418.2020.9386826

Zhang, J., Yang, R., & Zhang, C. (2019). High-Performance Low-Pass Filter Using Stepped Impedance Resonator and Defected Ground Structure. *Electronics*, *8*(4), 403. https://doi.org/10.3390/electronics8040403